Entangled Bessel-Gaussian beams

Melanie McLaren,[1,2] **Megan Agnew,**[3] **Jonathan Leach,**[3] **Filippus S. Roux,**[1] **Miles J. Padgett,**[4] **Robert W. Boyd,**[3,5] **and Andrew Forbes**[1,2*]

[1]*CSIR National Laser Centre, P.O. Box 395, Pretoria 0001, South Africa*
[2]*Laser Research Institute, University of Stellenbosch, Stellenbosch 7602, South Africa*
[3]*Department of Physics, University of Ottawa, 150 Louis Pasteur, Ottawa, Ontario, K1N 6N5 Canada*
[4]*Department of Physics and Astronomy, SUPA, University of Glasgow, Glasgow, UK*
[5]*Institute of Optics, University of Rochester, Rochester, new York 14627, USA*
[*]*Corresponding author: aforbes1@csir.co.za*

Abstract: Orbital angular momentum (OAM) entanglement is investigated in the Bessel-Gaussian (BG) basis. Having a readily adjustable radial scale, BG modes provide an alternative basis for OAM entanglement over Laguerre-Gaussian modes. We show that the OAM bandwidth in terms of BG modes can be increased by selection of particular radial wavevectors and leads to a flattening of the spectrum, which allows for higher dimensionality in the entangled state. We demonstrate entanglement in terms of BG modes by performing a Bell-type experiment and showing a violation of the Clauser-Horne-Shimony-Holt inequality for the $\ell = \pm 1$ subspace. In addition, we use quantum state tomography to indicate higher-dimensional entanglement in terms of BG modes.

OCIS codes: (270.0270) Quantum optics; (230.6120) Spatial light modulators.

References and links

1. H. Arnaut and G. Barbosa, "Orbital and intrinsic angular momentum of single photons and entangled pairs of photons generated by parametric down-conversion," Phys. Rev. Lett. **85**, 286–289 (2000).
2. Franke-Arnold, S. S. Barnett, M. Padgett, and L. Allen, "Two-photon entanglement of orbital angular momentum states," Phys. Rev. A **65(3)**, 033823 (2002).
3. A. Mair, A. Vaziri, G. Weihs, and A. Zeilinger, "Entanglement of the orbital angular momentum states of photons," Nature **412**, 313–316 (2001).
4. T. Pittman, Y. Shih, D. Strekalov, and A. Sergienko, "Optical imaging by means of two-photon quantum entanglement," Phys. Rev. A **52**, R3429–R3432 (1995).
5. A. Ekert, "Quantum cryptography based on Bells theorem," Phys. Rev. Lett. **67**, 661–663 (1991).
6. N. Gisin, G. Ribordy, W. Tittel, and H. Zbinden, "Quantum cryptograpy," Rev. Mod. Phys. **74**, 145–195 (2002).
7. M. Nielsen and I. Chuang, *Quantum Computation and Quantum Information* (Cambridge University Press, Cambridge, England, 2000).
8. V. Salakhutdinov, E. Eliel, and W. Löffler, "Full-field quantum correlations of spatially entangled photons," Phys. Rev. Lett. **108**, 173604 (2012).
9. L. Allen, M. Beijersbergen, R. Spreeuw, and J. Woerdman, "Orbital angular momentum of light and the transformation of Laguerre-Gaussian laser modes," Phys. Rev. A **45**, 8185–8189 (1992).
10. J. Durnin, "Exact solutions for nondiffracting beams. i. the scalar theory," J. Opt. Soc. Am. A **4**, 651–654 (1987).
11. J. Durnin, J. Miceli Jr., and J. Eberly, "Diffraction-free beams," Phys. Rev. Lett. **58**, 1499–1501 (1987).
12. F. Gori, G. Guattari, and C. Padovani, "Bessel-Gauss beams," Opt. Commun. **64**, 491–495 (1987).
13. M. Agnew, J. Leach, M. McLaren, F. Roux, and R. Boyd, "Tomography of the quantum state of photons entangled in high dimensions," Phys. Rev. A **84**, 062101 (2011).
14. D. James, P. Kwiat, W. Munro, and A. White, "Measurement of qubits," Phys. Rev. A **64**, 052312 (2001).
15. R.T. Thew, K. Nemoto, A.G. White, and W.J. Munro, "Qudit quantum-state tomography," Phys. Rev. A **66**, 012303 (2002).

#173626 - $15.00 USD Received 1 Aug 2012; revised 21 Sep 2012; accepted 22 Sep 2012; published 1 Oct 2012

16. V. Arrizon, "Optimum on-axis computer-generated hologram encoded into low-resolution phase- modulation devices," Opt. Lett. **28**, 2521–2523 (2003).
17. J. Leach, B. Jack, M. Ritsch-Marte, R. Boyd, A. Jha, S. Barnett, S. Franke-Arnold, and M. Padgett, "Violation of a Bell inequality in two-dimensional orbital angular momentum state-spaces," Opt. Express **17**, 8287–8293 (2009).
18. R. Grobe, K. Rzazewski, and J. Eberly, "Measure of electron-electron correlation in atomic physics," J. Phys. B-At. Mol. Opt. **27**, L503–L508 (1994).
19. A. Dada, J. Leach, G. Buller, M. Padgett, and E. Andersson, "Experimental high-dimensional two-photon entanglement and violations of the generalized Bell inequalities," Nat. Phys. **7**, 677–680 (2011).
20. A. Vaziri, J.W Pan, T. Jennewein, G. Weihs, and A. Zeilinger, "Concentration of higher-dimensional entanglement: Qutrits of photon orbital angular momentum," Phys. Rev. Lett. **91**, 227902 (2003).
21. J. Clauser, M. Horne, A. Shimony, and R. Holt, "Proposed experiment to test local hidden-variable theories," Phys. Rev. Lett. **23**, 880–884 (1969).
22. B. Jack, J. Leach, H. Ritsch, S. Barnett, and M. Padgett, "Precise quantum tomography of photon pairs with entangled orbital angular momentum," New J. of Phys. **811**, 103024 (2009).
23. S. Bose and V. Vedral, "Mixedness and teleportation," Phys. Rev. A **61**, 040101(R) (2000).
24. D. Collins, N. Gisin, N. Linden, S. Massar, and S. Popescu, "Bell inequalities for arbitrarily high-dimensional systems," Phys. Rev. Lett. **88**, 040404 (2002).

1. Introduction

The use of the orbital angular momentum (OAM) eigenstates of photons in quantum information science became attractive after it was shown, theoretically [1, 2] and experimentally [3], that OAM is conserved during spontaneous parametric down-conversion (SPDC) — the azimuthal indices of a pair of down-converted photons add up to that of the pump beam. As a result, the pair of down-converted photons are naturally entangled in terms of their azimuthal indices or OAM. Entanglement is a desirable property in quantum information applications, where it has been used in quantum ghost imaging [4], quantum cryptography [5, 6] and in quantum computing algorithms [7]. Any transverse spatial modal basis defines an infinite-dimensional Hilbert space, allowing more information per photon to be used in quantum information applications.

Although the Laguerre-Gaussian (LG) modes are currently the popular choice for theoretical analyses of quantum information systems based on OAM, the modal basis used in quantum information experiments are seldom pure LG modes; see Ref. [8]. The optical manipulation and detection of LG modes requires control of the radial index, which governs the radial shape of each LG mode's intensity profile. We shall refer to the modes that are detected without this radial control as azimuthal modes; in effect, azimuthal modes are thus defined by a Gaussian function modulated by a helical phase. The azimuthal index is not associated with a unique quantum state, but with a subspace of the total Hilbert space. If the radial part of the mode changes, a photon propagating through an optical system may suffer a loss of its quantum entanglement, even if the azimuthal index is unaffected. As the complexity of quantum information systems increases, the requirements for the fidelity of the quantum states can be expected to become more demanding.

Although the connection between the spatial modal profile of an optical beam and OAM was initially made with specific reference to LG beams [9], the same property applies to any optical beam with a rotationally symmetric intensity profile. As a result, Bessel beams [10, 11] and Bessel-Gaussian (BG) beams [12] also have quantized amounts of OAM associated with them. Each photon in such a beam also carries an amount of OAM equal to $\ell\hbar$, where ℓ is the azimuthal index of the mode.

In this paper, we investigate the use of BG modes [12] as a basis for photonic quantum information experiments. The radial index associated with LG modes is replaced by a continuous scaling parameter for the radial part of the BG modes. The relative ease and accuracy with which one can manipulate the azimuthal and radial dependencies of BG modes make them an

#173626 - $15.00 USD Received 1 Aug 2012; revised 21 Sep 2012; accepted 22 Sep 2012; published 1 Oct 2012

alternative choice for high-fidelity quantum information systems. In our study we measure the OAM spectrum of the quantum state produced by the SPDC process by projective measurements in the BG basis. We compare the high-dimensional density matrices measured in the BG basis to those measured in the azimuthal basis. Our results indicate that under the correct experimental conditions, the generation and measurement of high-dimensional entanglement in the BG basis is advantageous compared to the azimuthal basis.

2. Bessel-Gaussian Modes

The electric field of a BG mode is given by

$$\begin{aligned} E_\ell^{\mathrm{BG}}(r,\phi,z) &= \sqrt{\frac{2}{\pi}}\mathrm{J}_\ell\left(\frac{z_R k_r r}{z_R - iz}\right)\exp(i\ell\phi - ik_z z) \\ &\quad \times \exp\left(\frac{ik_r^2 z w_0^2 - 2kr^2}{4(z_R - iz)}\right) \end{aligned} \tag{1}$$

where ℓ is the azimuthal (mode) index (a signed integer); $\mathrm{J}_\ell(\cdot)$ is the Bessel function of the first kind; k_r and k_z are the transverse and longitudinal wave numbers, respectively. The initial radius of the Gaussian profile is w_0 and the Rayleigh range is $z_R = \pi w_0^2/\lambda$. It is clear from Eq. (1) that the radial component of the mode can be scaled by altering k_r.

The quantum state for the photon pairs produced in SPDC can be written in terms of BG modes,

$$|\Psi\rangle = \sum_\ell \int\int a_\ell(k_{r1},k_{r2})\,|\ell,k_{r1}\rangle_s\,|-\ell,k_{r2}\rangle_i\,\mathrm{d}k_{r1}\mathrm{d}k_{r2}, \tag{2}$$

where $|a_\ell(k_{r1},k_{r2})|^2$ denotes the probability for measuring a signal photon in state $|\ell,k_{r1}\rangle_s$ and an idler photon in state $|-\ell,k_{r2}\rangle_i$. In an experiment the radial scaling parameters k_{r1} and k_{r2} in Eq. (2) can be selected and adjusted in a continuous manner (see sec. 3) to optimize the bandwidth of the OAM spectrum.

If instead of integrating over k_{r1} and k_{r2} we select particular values, then the two-photon state for d dimensions can be written as

$$|\Psi(k_{r1},k_{r2})\rangle = \sum_\ell c_\ell\,|\ell\rangle_s\,|-\ell\rangle_i\,, \tag{3}$$

where ℓ ranges over d different values and c_ℓ represents the expansion coefficients. The sets of ℓ-values for different dimensions d are chosen as in Ref. [13]. Note that while the state after the SPDC process is anticorrelated in ℓ and thus spans d dimensions, the full state space has d^2 dimensions, because it also contains products of differing ℓ-values.

The density matrix of a two-photon qu*d*it quantum state can be reconstructed in terms of a Bloch representation,

$$\rho = \sum_{m,n=0}^{d^2-1} b_{m,n}\,\tau_m \otimes \tau_n, \tag{4}$$

where $b_{m,n}$ are complex coefficients with $b_{0,0} = 1/d^2$ for normalisation; τ_p are the d-dimensional generalised Gell-Mann matrices for $p = 1\ ...\ (d^2-1)$; τ_0 is the d-dimensional identity matrix. These coefficients are determined by performing a tomographically complete set of measurements. The quantum state in Eq. (2) consists of two qu*d*its, which results in a $d^2 \times d^2$ density matrix and thus requires approximately $d^4 - 1$ measurements to match the number of matrix elements [14, 15]. However, if an over-complete set of measurements is chosen,

#173626 - $15.00 USD Received 1 Aug 2012; revised 21 Sep 2012; accepted 22 Sep 2012; published 1 Oct 2012

additional information is available to compensate for measurement errors due to natural photon number fluctuations. An example of an over-complete set consists of the BG states $|\ell, k_r\rangle$ together with the superpositions of two BG states

$$|\alpha\rangle = \frac{1}{\sqrt{2}}\left[|\ell_1, k_r\rangle + \exp(i\alpha)|\ell_2, k_r\rangle\right]. \tag{5}$$

Here, α is the phase between the modes of the superposition states and k_r is chosen as a fixed value for all basis states.

3. Experimental Setup

Our experimental setup is shown in Fig. 1. A mode-locked laser source (Gaussian mode) with a wavelength of 355 nm and an average power of 350 mW was used to pump a 0.5-mm-thick type I BBO crystal to produce non-collinear, degenerate entangled photon pairs via SPDC. The plane of the crystal was imaged ($1.9\times$) by a $4f$ telescope onto two separate spatial light modulators (SLMs). The SLMs were used to select the particular pair of BG modes that were to be detected, as explained below. The SLM planes were re-imaged ($200\times$) by a $4f$ telescope and coupled into single-mode fibers to extract the pure Gaussian modal components. The fibers were connected to avalanche photodiodes, which then registered the photon pairs via a coincidence counter. The single count rates $S_\ell^{(s)}$ and $S_\ell^{(i)}$ were recorded simultaneously with the coincidence count rates C_ℓ and were accumulated over a 10 second integration time. An uncertainty from the pump beam fluctuations of 5% was observed for the measured coincidence counts.

In order to measure specific Bessel-Gauss modes, we use spatial light modulators and single mode fibers to perform a series of projection meaurements. The Bessel term of the hologram is encoded as a binary function that accounts for momentum conservation laws associated with the parametric downconversion process. The binary Bessel function is combined with a helical phase function that determines the azimuthal index ℓ of the detected BG mode. (Without the binary Bessel function, the transmission function is the same helical phase function that is traditionally used to measure azimuthal modes.) The binary encoding together with spatial filtering introduced by system apertures enables a projection mesurement that does not require complex amplitude modulation of the detected mode [16]. Consequently, the nature of the hologram ensures a high detection efficency of the entangled photons. The phase-only hologram used to project the photons into BG modes is given by the transmission function

$$T(r) = \text{sign}\left\{\mathrm{J}_\ell(k_r r)\right\}\exp(i\ell\phi), \tag{6}$$

where sign$\{\cdot\}$ denotes the sign-function, and the argument of Eq. (6) gives the desired function for the phase-only SLM. Not shown in Eq. (6) is an added blazed grating to select the 1st diffraction order (typically with an efficiency of approximately 60%). An image of the back-projected mode in the crystal plane, as determined by the hologram, is shown in the inset of Fig. 1, where the BG profile is clearly seen. Each azimuthal mode with a particular value of $|\ell\rangle$ is a superposition of different BG modes with the same azimuthal index, but different k_r values. The binary Bessel function, which is encoded on the SLMs, enables us to select a particular k_r value from this superposition. An error in k_r is determined by the resolution of the SLM (approximately 2%), 8 μm pitch and the width of the enveloping Gaussian beam (aprproxiamtely 1.5%). As a result of selecting one k_r family of BG modes, we anticipate that the spiral bandwidth of the spectrum will change depending on the chosen k_r value. The shape of the spectrum will change as a result of the binary Bessel function, because one only measures the part (one-dimensional slice) of the full two-dimensional spectrum that corresponds to a particular value of k_r. In the limit that k_r approaches zero, the scale of the Bessel function

#173626 - $15.00 USD Received 1 Aug 2012; revised 21 Sep 2012; accepted 22 Sep 2012; published 1 Oct 2012

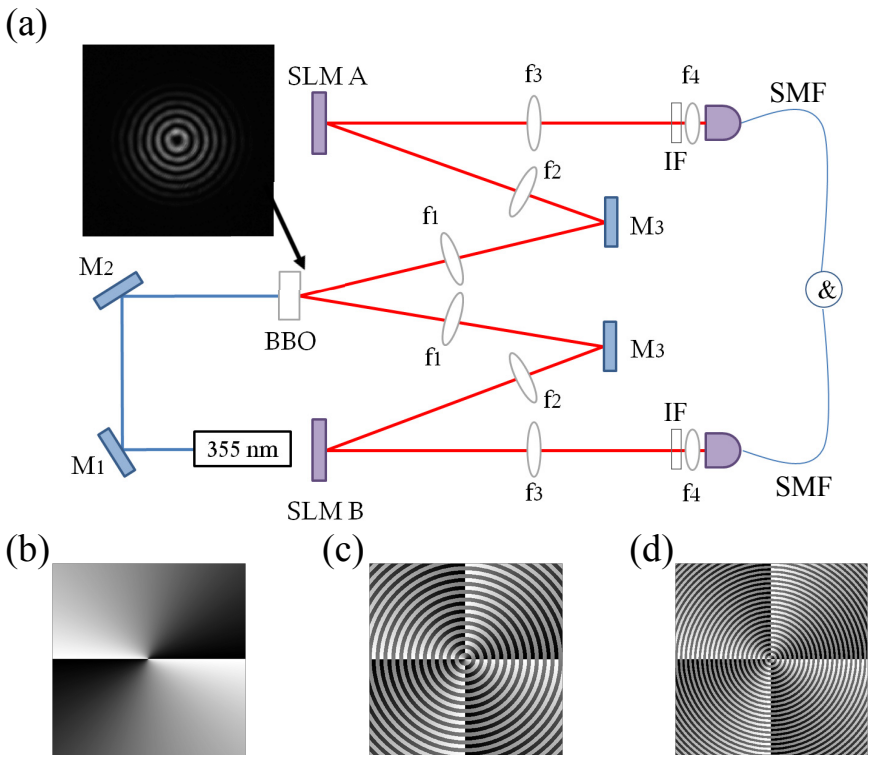

Fig. 1. (a) Experimental setup used to detect the OAM eigenstate after SPDC. The plane of the crystal was relayed imaged onto two separate SLMs using lenses, $f_1 = 400$ mm and $f_2 = 750$ mm, where the BG modes were selected. Lenses $f_3 = 300$ mm and $f_4 = 1.5$ mm were used to relay image the SLM planes through 10 nm bandwidth interference filters (IF) to the inputs of the single-mode fibres (SMF). Examples of a phase-only binary Bessel hologram with a helical phase of $\ell = 2$ for different values of k_r are shown in (b) $k_r = 0$ rad/mm, (c) $k_r = 21$ rad/mm and (d) $k_r = 35$ rad/mm. The inset (at BBO crystal) shows a back-projected CCD image of a binary Bessel mode with helical phase $\ell = 2$ and radial wavevector $k_r = 21$ rad/mm measured at the plane of the crystal.

becomes larger than the Gaussian envelope. As a result the transmission function corresponds to that of an azimuthal mode.

Following the method derived in Ref. [17], we used superpositions of OAM states with $\pm\ell$, in analogy to the polarisation states, to demonstrate the violation of a Bell-type inequality for the $\ell = \pm 1$ subspace. The superposition states for BG modes given by Eq. (5) were oriented at angles α_A and α_B for the signal and idler photons, respectively.

Using the method described in Ref. [13], we calculate the density matrix for higher dimensions by minimizing the Chi-square quantity,

$$\chi^2 = \sum_{i=1}^{N^2} \frac{\left[p_i^{(M)} - p_i^{(P)}\right]^2}{p_i^{(P)}}, \tag{7}$$

where $p_i^{(M)}$ are the normalized coincident counts, which are interpreted as experimentally measured probabilities, and $p_i^{(P)}$ are the predicted probabilities calculated from the density matrix. We construct the density matrix so that it is both Hermitian and positive semi-definite with

#173626 - $15.00 USD Received 1 Aug 2012; revised 21 Sep 2012; accepted 22 Sep 2012; published 1 Oct 2012

unitary trace [14]. This is necessary as the effects of statistical variations of the coincidence count rates and experimental inaccuracies commonly produce reconstructed density matrices with negative eigenvalues and a non-unitary trace.

4. Experimental Results

In the first experiment we vary the radial wave number k_r on each SLM and monitor the coincidence counts for each ℓ mode. For $k_r = 0$ the phase functions on the SLMs consist of only the helical phase. As a result the $k_r = 0$ measurements correspond to the conventional azimuthal modal spectrum. The OAM bandwidth can be quantified as the standard deviation (square root of the second moment) in ℓ, given by

$$B = \left[\frac{\sum_{\ell} \ell^2 C_\ell(k_r)}{\sum_{\ell} C_\ell(k_r)} \right]^{1/2} \tag{8}$$

which is a measure of the width of the spectrum, or as the Schmidt number [18]

$$K = \frac{\left[\sum_{\ell} C_\ell(k_r) \right]^2}{\sum_{\ell} C_\ell^2(k_r)}. \tag{9}$$

Both quantities are plotted as a function of k_r in Fig. 2(a). These results both point to an increased number of modes participating in the entangled state.

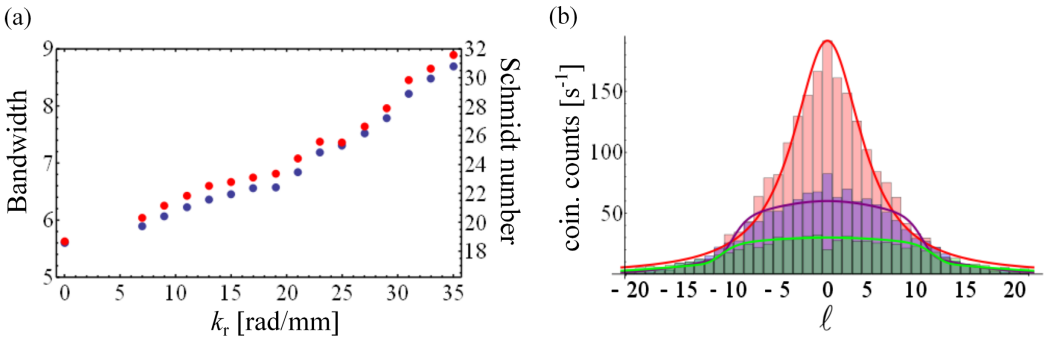

Fig. 2. (a) OAM bandwidth (blue) and Schmidt number (red) are shown as a function of k_r. As the radial wavevector increases from $k_r = 0$ rad/mm (azimuthal modes), the OAM bandwidth increases. (b) OAM spectrum for azimuthal modes (red) and BG modes for $k_r = 21$ rad/mm (purple) and $k_r = 35$ rad/mm (green), in terms of the modal weightings. The maximum coincidence count rate is lower for both BG modes; however a broader spectrum is observed with increasing k_r.

We observe almost a doubling in the OAM bandwidth from $k_r = 0$ rad/mm (azimuthal modes) to $k_r = 35$ rad/mm (BG modes). This tuneability in the radial component of the field allows for the OAM spectrum to be customised through application of Eq. (2). In Fig. 2(b) one can observe the broadening of the OAM spectrum as the k_r is increased from $k_r = 0$ rad/mm (red) to $k_r = 21$ rad/mm (purple) to $k_r = 35$ rad/mm (green). The maximum coincidence count rate decreases for BG modes, but its spectrum is broader than that of the azimuthal modes. The full-width half-maximum (FWHM) widths of the spectra indicate that the BG modal spectrum

#173626 - $15.00 USD Received 1 Aug 2012; revised 21 Sep 2012; accepted 22 Sep 2012; published 1 Oct 2012

at $k_r = 35$ rad/mm is almost twice as wide as the azimuthal modal spectrum obtained at $k_r = 0$. The wider bandwidth and flatter spectrum is indicative of the initial spectrum produced by the SPDC process. The reduction in the central region of the spectrum makes Procrustean filtering in higher-dimensional entanglement experiments [19] unnecessary. Our results could also be interrupted as a form of entanglement concentration [20], where maximally entangled states are extracted from non-maximally entangled pure states. Beyond a certain ℓ-value, the BG spectrum coincides with the azimuthal modal spectrum. This can be understood as a consequence of having a large ℓ-value with a fixed-width Gaussian envelope: the Gaussian suppression of the function beyond a certain radius causes the definition of the radial dependence of the mode for large ℓ-values to have little or no effect. Although the spatial resolution of the SLMs would become a limiting factor, larger values of k_r are expected to give OAM spectra with larger bandwidths. The wider bandwidth allows more basis states to be incorporated in quantum information systems.

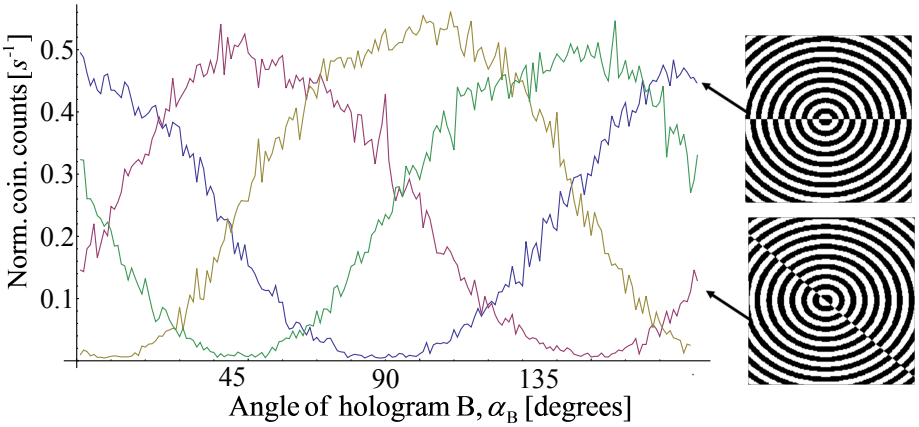

Fig. 3. Sinusoidal behaviour of the normalised coincidence counts as a function of the angular position of the holograms, for $\ell = \pm 1$ subspace at positions $\alpha_A = 0°$ (blue), 45° (pink), 90° (green) and 135° (yellow). The insets show the holograms used for $\alpha_A = 0°$ and $\alpha_A = 45°$, where the phase varies from 0 (black) to π (white).

To verify that the quantum state produced in the SPDC process is entangled, we use it to test a Bell-type inequality. Clauser, Horne, Shimony and Holt (CHSH) provided a method to test Bell's theorem experimentally, stating that no local hidden-variable theory could simulate the kind of statistical predictions made by quantum mechanics [21]. We fixed α_A from Eq. (5) at four different angles: $\alpha_A = 0°, 45°, 90°, 135°$, allowing α_B to vary continuously from 0° to 180°. The Bell parameter, as defined in Ref. [17], is given by

$$S = E(\alpha_A, \alpha_B) - E(\alpha_A, \alpha'_B) + E(\alpha'_A, \alpha_B) - E(\alpha'_A, \alpha'_B), \tag{10}$$

where

$$E(\alpha_A, \alpha_B) = \frac{C(\alpha_A, \alpha_B) + C(\alpha_A + \frac{\pi}{2\ell}, \alpha_B + \frac{\pi}{2\ell}) - C(\alpha_A + \frac{\pi}{2\ell}, \alpha_B) - C(\alpha_A, \alpha_B + \frac{\pi}{2\ell})}{C(\alpha_A, \alpha_B) + C(\alpha_A + \frac{\pi}{2\ell}, \alpha_B + \frac{\pi}{2\ell}) + C(\alpha_A + \frac{\pi}{2\ell}, \alpha_B) + C(\alpha_A, \alpha_B + \frac{\pi}{2\ell})}, \tag{11}$$

with $C(\alpha_A, \alpha_B)$ being the coincidence count rate for the particular orientation of each hologram. The Bell curves are shown in Fig. 3 for BG modes with $k_r = 21$ rad/mm. For the two-dimensional BG subspace of $\ell = 1$, we find the Bell parameter in the CHSH inequality to be $S = 2.78 \pm 0.05 > 2$, which violates the inequality by 15 standard deviations.

#173626 - $15.00 USD Received 1 Aug 2012; revised 21 Sep 2012; accepted 22 Sep 2012; published 1 Oct 2012

We also reconstructed the (two-dimensional) two-photon density matrix, as shown in Fig. 4(a), in the BG basis for $k_r = 21$ rad/mm and $\ell = \pm 1$, using a full quantum state tomography [22]. The purity of the state $\mathrm{Tr}(\rho^2)$ was calculated as 0.981, where its closeness to 1 indicates that the observed quantum state is close to a pure state. To quantify the mixture of the measured state we calculate the linear entropy [23] $S_L = 4/3[1 - \mathrm{Tr}(\rho^2)]$. We find the linear entropy of our quantum state to be $S_{L2} = 0.06 \pm 0.01$, indicating that our state is close to a pure state (the linear entropy for a pure state is zero, whereas a completely mixed state is charaterised by a linear entropy of one).

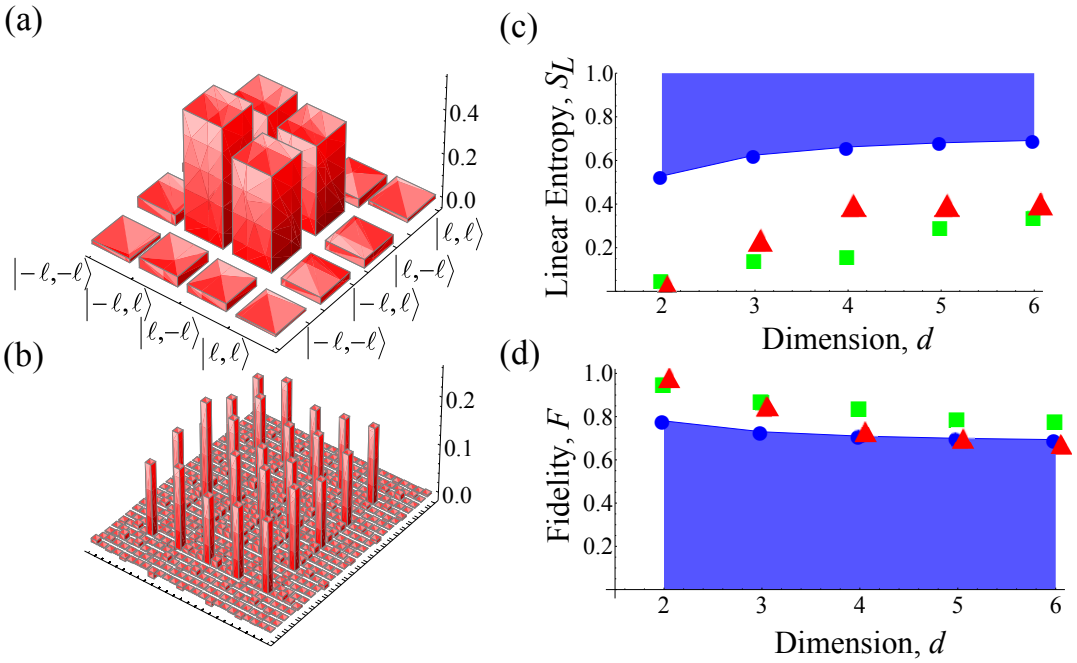

Fig. 4. Results from a full quantum state tomography of a BG mode with $k_r = 21$ rad/mm. (a) & (b) Graphical representation of the real part of the density matrix for dimension $d = 2$ and $d = 5$, respectively. (c) Linear entropy and (d) fidelity as a function of dimension. The red triangles represent the measured data for the azimuthal modes, the green squares represent the measured data for the BG modes and the blue circles represent the threshold states in Eq. (13).

We also calculate the fidelity

$$F = \left[\mathrm{Tr}\left\{(\sqrt{\rho_T}\rho_d\sqrt{\rho_T})^{1/2}\right\}\right]^2, \tag{12}$$

which is a measure of how close our reconstructed state ρ_d is to the target state $\rho_T = |\psi_T\rangle\langle\psi_T|$. In our case the target state is the (pure) maximally entangled state, $|\psi_T\rangle = 2^{-1/2}(|\ell\rangle_s|-\ell\rangle_i + |-\ell\rangle_s|\ell\rangle_i)$. We find a fidelity of $F = 0.96 \pm 0.01$. These results are indicative of entanglement of our BG modes.

We performed high-dimensional state tomography measurements [13] from $d = 2$ to $d = 6$. For $d = 2$ we use the OAM basis states $|\ell\rangle = \pm 1$ to measure the probabilities for each pure state [Eq. (3)] and the superpositions [Eq. (5)] thereof. The superposition states are rotated by and angle of $\alpha = \pi/2$ such that the phase between the modes assumes values of $\{0, \pi/2, \pi, 3\pi/2\}$. Similarly for $d = 3$ we include the states $|\ell\rangle = \{-1, 0, 1\}$, up to $d = 6$

#173626 - $15.00 USD Received 1 Aug 2012; revised 21 Sep 2012; accepted 22 Sep 2012; published 1 Oct 2012

with the states $|\ell\rangle = \{-3,-2,-1,1,2,3\}$. Using the measurement probabilities we calculated a higher-dimensional density matrix (real part) for $d = 5$ in Fig. 4(b). The constructed density matrices were used to compute the linear entropy and fidelity, with the results shown in Figs. 4(c) and (d), respectively. We found that the higher-dimensional quantum states in terms of the BG modes for a particular k_r have higher entanglement (high fidelity) than the quantum states in terms of azimuthal modes, while remaining relatively pure (low linear entropy), as shown in Fig. 4(c) and (d). These measurements are compared with the threshold states, which are given by

$$\rho_B = \mathrm{p}_d^{min} |\psi\rangle \langle\psi| + (1 - \mathrm{p}_d^{min}) \frac{I}{d^2}, \tag{13}$$

which lie on the threshold of the high-dimensional Bell inequality [24]. Here p_d^{min} is the probability above which the Bell inequality is violated, I is the identity matrix of dimension d^2 and $|\psi\rangle$ is the maximally entangled state of two d-dimensional systems [24]. The fidelity values ranged from $F_2 = 0.96 \pm 0.01$ to $F_6 = 0.79 \pm 0.01$ for the BG modes, while the values for linear entropy were found to be $S_{L2} = 0.06 \pm 0.01$ and $S_{L6} = 0.35 \pm 0.01$.

5. Discussion and Conclusion

We have successfully demonstrated that BG modes are entangled in the high-dimensional OAM degree of freedom. Crucially, the ability to select the radial component allows us to record BG states with a very broad spiral spectrum. The resulting high-dimensionally entangled states are closer to the appropriate maximally entangled state compared to azimuthal modes. Such control of the experimental conditions results in a higher information capacity per photon pair and allows for more states to be utilized in quantum information processes. The only cost of the increased spiral spectrum of the recorded modes is a lower coincidence count rate. Due to the particular interference properties of BG modes, entangled modes in this basis may offer increased robustness when propagating through turbulent media. The finite space-bandwidth product of the SLMs limits the achievable spectrum of the BG modes; however, alternative methods may offer further improvements in OAM entanglement with BG modes.

Acknowledgments

The authors gratefully acknowledge support from various funding agencies as follows: MA, JL, and RWB from the Canada Excellence Research Chairs program; RWB from the US DARPA InPho program; MJP from US DARPA InPho program and the Royal Society; MM, AF and FSR from the NRF and the CSIR.

#173626 - $15.00 USD Received 1 Aug 2012; revised 21 Sep 2012; accepted 22 Sep 2012; published 1 Oct 2012